



UNIVERSITY OF LEEDS

This is a repository copy of *In situ and time resolved nucleation and growth of silica nanoparticles forming under simulated geothermal conditions*.

White Rose Research Online URL for this paper:
<http://eprints.whiterose.ac.uk/80235/>

Version: Accepted Version

Article:

Tobler, DJ and Benning, LG (2013) In situ and time resolved nucleation and growth of silica nanoparticles forming under simulated geothermal conditions. *Geochimica et Cosmochimica Acta*, 114. 156 - 168. ISSN 0016-7037

<https://doi.org/10.1016/j.gca.2013.03.045>

Reuse

Unless indicated otherwise, fulltext items are protected by copyright with all rights reserved. The copyright exception in section 29 of the Copyright, Designs and Patents Act 1988 allows the making of a single copy solely for the purpose of non-commercial research or private study within the limits of fair dealing. The publisher or other rights-holder may allow further reproduction and re-use of this version - refer to the White Rose Research Online record for this item. Where records identify the publisher as the copyright holder, users can verify any specific terms of use on the publisher's website.

Takedown

If you consider content in White Rose Research Online to be in breach of UK law, please notify us by emailing eprints@whiterose.ac.uk including the URL of the record and the reason for the withdrawal request.



eprints@whiterose.ac.uk
<https://eprints.whiterose.ac.uk/>

Manuscript Number:

Title: In situ and time resolved nucleation and growth of silica nanoparticles forming under simulated geothermal conditions

Article Type: Article

Corresponding Author: Dr. Dominique J Tobler,

Corresponding Author's Institution:

First Author: Dominique J Tobler

Order of Authors: Dominique J Tobler; Liane G Benning

Abstract: Detailed knowledge of the reaction kinetics of silica nanoparticles formation in cooling supersaturated waters is fundamental to the understanding of many natural processes including biosilicification, sinter formation, and silica diagenesis. Here, we quantified the formation of silica nanoparticles from solution as it would occur in geothermal waters. We used an in situ and real-time approach with silica polymerisation being induced by fast cooling of a 230°C hot and supersaturated silica solution. Experiments were carried out using a novel flow-through geothermal simulator system that was designed to work on-line with either a synchrotron-based small angle X-ray scattering (SAXS) or a conventional dynamic light scattering (DLS) detector system. Our results show that the rate of silica nanoparticle formation is proportional to the silica concentration (640 vs. 960 ppm), and the first detected particles form spheres of approximately 3 nm in diameter. These initial nanoparticles grow and reach a final particle diameter of approximately 7 nm. Interestingly, neither variations in ionic strength (0.02 vs. 0.06) nor temperature (reactions at 30 to 60°C, mimicking Earth surface values) seem to affect the formation kinetics or the final size of the silica nanoparticles formed. Comparing these results with our previous data from experiments where silica polymerisation and nanoparticle formation was induced by a drop in pH from 12 to near neutral [pH-induced, Tobler D.J., Shaw S. and Benning L.G. (2009) Quantification of initial steps of nucleation and growth of silica nanoparticles: an in-situ SAXS and DLS study. *Geochim. Cosmochim. Acta* 73, 5377-5393] showed that (a) the mechanisms and kinetics of silica nanoparticle nucleation and growth were unaffected by the means to induce silica polymerisation (T drop or pH drop), both following first order reactions kinetics coupled with a surface controlled reaction mechanism. However, the rates of the formation of silica nanoparticles were substantially (around 50 %) slower when polymerisation was induced by fast cooling as opposed to pH change. This was evidenced by the occurrence of an induction period, the formation of larger critical nuclei, and the absence of particle aggregation in the T - induced experiments.

Corresponding Author: Dr Dominique J. Tobler

School of Geographical and Earth Sciences

Gregory Building, University of Glasgow

G12 8QQ, Leeds, UK

dominique.tobler@glasgow.ac.uk

Phone: (+44) 141 330 5442

Fax: (+44) 141 330 4817

June 19th, 2012

Dear Editor

Enclosed please find our manuscript "In situ and time resolved nucleation and growth of silica nanoparticles forming under simulated geothermal conditions" by Dominique J. Tobler and Liane G. Benning. This paper describes a comprehensive, original laboratory study which had the main goal to quantify the initial steps of silica polymerisation and silica nanoparticle formation in cooling silica saturated solutions that mimicked the processes observed in geothermal systems using synchrotron-based Small Angle X-ray Scattering and conventional Dynamic Light Scattering (DLS) combined with Scanning and Transmission Electron Microscopy.

This work has not been published elsewhere, wholly or in part, and is not and will not be submitted elsewhere for publication while it is in review for GCA. Both authors have seen the manuscript and agree to its submission to GCA. Three suggested associate editors and six potential reviewers are added below.

Yours sincerely

A handwritten signature in black ink, appearing to read 'Dominique Tobler', with a long horizontal flourish extending to the left.

Dominique Tobler

Suggested associate editors:

C. Kim

School of Earth and Environmental Sciences, Chapman University, Orange, CA 92866, USA

J. Chorover

Department of Soil, Water and Environmental Science, University of Arizona, Box 210038, Tucson, AZ 85721-0038, USA
University of Delaware, Newark, DE, USA

C.J. Daughney

Institute of Geological and Nuclear Sciences, Wellington, New Zealand

Suggested reviewers:

Carole C. Perry

The Nottingham Trent University, Department of Chemistry and Physics, Nottingham, NG11 8NS, UK, phone: +44 115 848 669, carole.perry@ntu.ac.uk

Gary Icopini

Montana Tech of The University of Montana, 1300 West Park Street, Butte, MT 59701, phone: (406) 496-4841, gicopini@mtech.edu

Susan A. Carroll

Lawrence Livermore National Laboratory, P.O. Box 808, Livermore, CA 94551, USA, phone: 925-423-5694, carroll6@llnl.gov

Jean Pierre Jolivet

UMR CNRS 7574, Université Pierre et Marie Curie, Collège de France, 11 place Marcelin Berthelot, 75231 Paris, jean-pierre.jolivet@upmc.fr

Claudine Chopin-Noguera

L'Institut des Nano-Sciences de Paris (INSP), 4 place Jussieu, boîte courrier 840 75252 PARIS cedex 05, noguera@insp.jussieu.fr

Peter Bots

Research Centre for Radwaste and Decommissioning, The 596 University of Manchester, Manchester M13 9PL, U.K. pieter.bots@manchester.ac.uk

1 **In situ and time resolved nucleation and growth of silica nanoparticles**
2 **forming under simulated geothermal conditions**

3

4 Dominique J. Tobler¹ (Corresponding Author^{*}) and Liane G. Benning¹

5

6

7 1 Earth and Biosphere Institute, School of Earth and Environment, University of Leeds, LS2 9JT, Leeds,
8 UK

9

10

11

12 * Present address: School of Geographical and Earth Sciences, University of Glasgow, Gregory Building,
13 G12 8QQ, Glasgow, UK (dominique.tobler@glasgow.ac.uk)

14

15 Phone: +44 141 330 5442

16 Fax: +44 141 330 4817

17

ABSTRACT

1
2 Detailed knowledge of the reaction kinetics of silica nanoparticles formation in cooling supersaturated
3 waters is fundamental to the understanding of many natural processes including biosilicification, sinter
4 formation, and silica diagenesis. Here, we quantified the formation of silica nanoparticles from solution as
5 it would occur in geothermal waters. We used an in situ and real-time approach with silica polymerisation
6 being induced by fast cooling of a 230°C hot and supersaturated silica solution. Experiments were carried
7 out using a novel flow-through geothermal simulator system that was designed to work on-line with either
8 a synchrotron-based small angle X-ray scattering (SAXS) or a conventional dynamic light scattering
9 (DLS) detector system. Our results show that the rate of silica nanoparticle formation is proportional to
10 the silica concentration (640 vs. 960ppm), and the first detected particles form spheres of approximately 3
11 nm in diameter. These initial nanoparticles grow and reach a final particle diameter of approximately 7
12 nm. Interestingly, neither variations in ionic strength (0.02 vs. 0.06) nor temperature (reactions at 30 to
13 60°C, mimicking Earth surface values) seem to affect the formation kinetics or the final size of the silica
14 nanoparticles formed. Comparing these results with our previous data from experiments where silica
15 polymerisation and nanoparticle formation was induced by a drop in pH from 12 to near neutral [pH-
16 induced, Tobler D.J., Shaw S. and Benning L.G. (2009) Quantification of initial steps of nucleation and
17 growth of silica nanoparticles: an in-situ SAXS and DLS study. *Geochim. Cosmochim. Acta* 73, 5377-
18 5393] showed that (a) the mechanisms and kinetics of silica nanoparticle nucleation and growth were
19 unaffected by the means to induce silica polymerisation (T drop or pH drop), both following first order
20 reactions kinetics coupled with a surface controlled reaction mechanism. However, the rates of the
21 formation of silica nanoparticles were substantially (around 50 %) slower when polymerisation was
22 induced by fast cooling as opposed to pH change. This was evidenced by the occurrence of an induction
23 period, the formation of larger critical nuclei, and the absence of particle aggregation in the T - induced
24 experiments.

1. INTRODUCTION

1
2 The polymerisation of aqueous silica leading to the formation of silica nanoparticles occurs in many
3 natural environments (e.g., hot springs, diatoms, marine sediments) and is critical to a variety of processes
4 including biosilicification, biomineralisation, silica diagenesis, or silica sinter formation. Nevertheless,
5 the mechanisms and kinetics by which silica nanoparticles form, grow and aggregate are still fragmented.
6 Several studies investigated the rates of silica polymerization and silica precipitation in solutions that
7 mimicked natural fluids (e.g., Iler, 1979; Rothbaum and Rhode, 1979; Rimstidt and Barnes, 1980; Conrad
8 et al., 2007; Tobler et al., 2009 and references therein), thereby obtaining a better understanding of the
9 parameters that control silica saturation in natural waters. In these studies, physico-chemical factors
10 including solution pH, temperature, ionic strength, and silica concentration were shown to heavily
11 influence the degree of silica saturation and thus the kinetics of silica polymerisation and bulk
12 precipitation.

13 Despite the fact that these studies have provided us with a basic understanding of how silica polymerises,
14 little research has so far focused on the nucleation and growth kinetics or the mechanisms that lead to the
15 formation of nanocolloidal silica particles from supersaturated solutions under conditions that mimic
16 natural waters. These initial steps in the polymerisation and precipitation reaction are however, most
17 important as they determine the size, shape and composition of the nanoparticles, and ultimately define
18 their reactivity (i.e., catalysts; uptake of nutrients / contaminants) and transport behaviour (if the
19 nanoparticles remain in suspension) as well as the ultimate structure and texture of the forming
20 precipitates (e.g., sinters in geothermal waters). For example, sinter growth studies (e.g., Mountain et al.,
21 2003; Handley et al. 2005; Tobler et al., 2008, Tobler and Benning, 2011) indicated that the success and
22 failure of microbial silicification and fossilization greatly depended on sinter growth rates, and these in
23 turn rely on the quantitative assessment of the kinetics and mechanisms of silica nanoparticle nucleation
24 and growth processes.

1 So far, most experimental studies on nanocolloidal silica focused on the synthesis of highly
2 monodisperse, spherical and compact silica particles through techniques such as the Stöber method
3 (Stöber et al., 1968). This method uses organic alkoxides precursors as reactants for the production of
4 large quantities of highly size controlled and monodispersed silica nanoparticles for a multitude of
5 industrial application (e.g., biotechnology, catalysis and chromatography). In these alkoxide based
6 synthesis studies, various techniques including small angle X-Ray scattering (SAXS), dynamic light
7 scattering (DLS), transmission electron microscopy (TEM), and Raman spectroscopy have been used to
8 derive rates of polymerisation and rates of silica nanoparticle formation (e.g., Halasz et al., 2011; Pabisch
9 et al., 2012). It is however, worth noting that the Stöber method, with its alkoxide-based chemical starting
10 materials and the highly monodispersed final silica nanoparticles, is not representative of silica
11 nanoparticle formation in any natural environment and thus the derived kinetic models are not
12 transferable to any natural process.

13 To date, only few attempts were made to quantify the shapes, sizes or kinetics of silica nanoparticles
14 forming in fluids of geologic significance (e.g., Iler, 1979; Rothbaum and Rhode, 1979; Makrides et al.,
15 1980; Conrad et al., 2007; Tobler et al. 2009 and references therein). Amongst these, only our previous
16 study focused on the nucleation and growth kinetics and mechanisms of the silica nanoparticles
17 themselves and used the changes in aqueous silica chemistry (polymerisation rates) primarily as a cross-
18 confirmative measure. In Tobler et al. (2009) we showed that at ambient conditions, when silica
19 supersaturation is induced by a pH change, the nucleation and growth of silica nanoparticles follows three
20 stages: (1) Nucleation: characterized by instantaneous homogeneous nucleation where monosilicic acid
21 polymerises to form stable critical nuclei having a diameter of 1–2 nm; (2) 3-D growth: characterized by
22 silica nanoparticles growth following first order reaction kinetics coupled with a surface-controlled
23 reaction mechanism; (3) Ostwald ripening and particle aggregation.

24 In this current study, we build upon our previous work with the aim to better mimic processes in the
25 natural world (i.e., geothermal systems) including investigating the effect of fast cooling of a silica

1 supersaturated solution on silica polymerisation and silica nanoparticles growth. This is in contrast to
2 most previous studies, where silica polymerisation was most often induced by neutralising a
3 supersaturated, high-pH (usually pH 12 or higher) silica solution to near neutral values in order to bring
4 silica solubility to its minimum (Alexander et al., 1954). However, in most natural systems (e.g.,
5 geothermal pools or deep-sea vents) silica polymerisation and silica nanoparticle formation is the result of
6 cooling (often extremely fast) of a high-temperature, silica supersaturated near-neutral fluid to ambient
7 (geothermal) or low temperatures (deep sea) rather than a drastic pH change. A few studies (e.g.,
8 Rothbaum and Rhode, 1979; Weres, 1981; Carroll et al., 1998) have indicated that silica polymerisation is
9 delayed in systems where silica supersaturation is induced by fast cooling, but so far a direct comparison
10 and a quantitative assessment of the differences in silica nanoparticle nucleation and growth kinetics and
11 mechanisms between these two approaches is missing. This is mainly due to divergent experimental set-
12 ups used in field vs. lab studies (e.g., usage of silica gels, quantifying total silica scale) as well as
13 differences in the evaluation of the reaction kinetics (e.g., precipitation rate as a function of the Gibbs free
14 energy of reaction or as a function of aqueous silica polymerisation rates with varying reaction orders).
15 Furthermore, so far the experimental challenges in mimicking such reactions in the laboratory (e.g.,
16 running hydrothermal flow through simulators, controlling the fast cooling while simultaneously
17 monitoring the nucleation/growth kinetics etc.) precluded the quantification of the kinetics and
18 mechanisms of silica nanoparticles formation from cooling hot fluids.

19 In this current study, we used a flow-through geothermal simulator system that was optimized to operate
20 in conjunction with either a synchrotron-based small angle X-ray scattering (SAXS) system or a
21 conventional flow-through dynamic light scattering (DLS) set-up (Fig. 1). Both these approaches allowed
22 us, independently of each other, to quantify the in-situ and in real-time nucleation and growth of silica
23 nanoparticles from high temperature solutions. This was done with silica supersaturation being reached
24 through the fast cooling of hot fluids, thus accurately mimicking a natural geothermal system where hot
25 silica supersaturated solutions emerge as springs at the Earth's surface forming amorphous silica sinter

1 deposits (e.g., Carroll et al., 1998; Konhauser et al., 2001; Mountain et al., 2003; Handley et al., 2005;
2 Tobler et al. 2008). In all our experiments the in situ scattering data were complemented by aqueous
3 chemical and electron microscopic imaging data, which cross-confirmed the rates, sizes and
4 polydispersity of the nucleating and growing silica nanoparticles. The reactions were monitored for a
5 range of silica concentrations ($[\text{SiO}_2]$), ionic strengths (IS) and temperatures and results were compared to
6 our previous data from experiments where the polymerisation reaction was triggered by a pH-drop
7 (Tobler et al., 2009).

8

9

2. METHODOLOGY

10 2.1 Experimental set-up and silica nanoparticle synthesis

11 The flow-through geothermal simulator and the in-line reaction cells/detector systems are illustrated in
12 Figure 1. A supersaturated solution with a total silica concentration $[\text{SiO}_2]$ of either 640 or 960ppm, and
13 an ionic strength (IS) of 0.02 or 0.06 was prepared at ambient temperatures (25°C) in a 10 L storage bottle
14 by dissolving specific amounts of $\text{Na}_2\text{SiO}_2 \cdot 5\text{H}_2\text{O}$ and NaCl in deionised water. Adjusting the pH of these
15 highly alkaline solutions (pH ~ 12) to 7 using 1M HCl lead to a partly polymerised, near neutral solution
16 (Fig. 1). To run an experiment, these solutions were pumped from the storage bottle into a high-
17 temperature oven (at 230°C) via a HPLC pump (Fig. 1). Inside the oven, the fluids passed through a 6 m
18 stainless steel coil. The high temperature and the approximately 2.5 h residence time (inside the oven)
19 caused the silica in the circulating fluid to fully de-polymerise, producing a monomeric silica solution
20 (i.e., all silica present as monosilicic acid, $[\text{SiO}_2(\text{aq})]$). This approach mimicked silica-rich fluids in the
21 Earth's crust at about 2-3 km depth and under hydrostatic pressures. After the silica solution passed
22 through the steel coil, it emerged from the oven and passed through a backpressure regulator (BPR)
23 located approximately 15 cm away from the oven exit. This distance assured a temperature drop from

1 230°C to ~80°C within <1 min. Critically, this induced an increase in silica supersaturation and thus
2 initiated silica polymerisation. Such a rapid cooling process simulated the conditions when a
3 supersaturated hot spring fluid is discharged at the Earth's surface (i.e., in a hot spring) and silica
4 polymerisation is initiated.

5 This geothermal simulator allows the in situ and time-resolved monitoring of the very first steps of
6 polymerisation and subsequent nucleation and growth of silica nanoparticles within a cooling solution. To
7 monitor these processes the outlet of the BPR is connected to a flow through quartz capillary SAXS cell
8 (1.5 mm OD and 10 µm walls) or a disposable plastic cuvette stationary in the DLS instrument via 1/8
9 inch Teflon tubing. Once each cell was full, the flow was stopped and data acquisition started (i.e.,
10 stopped-flow experiments). SAXS measurements were carried out at 30°C, while DLS measurements the
11 were run at final temperatures from 30 to 60°C. These varying final temperatures could be achieved by
12 adjusting the tubing length between the backpressure regulator and the SAXS and DLS cell, respectively
13 (i.e., cooling time). Both SAXS and DLS experiments were carried out for up to 3 hours with in situ
14 monitoring of the changes in the respective scattering properties.

15 Simultaneously with the SAXS/DLS data collection that monitored the growth of the silica nanoparticles,
16 the polymerisation of the aqueous silica was quantified via the time-dependent change in monosilicic acid
17 concentrations in the reacting solutions. About 5 ml of each cooling polymerising solution (collected from
18 the BPR outlet) was analyzed over time (up to 2 hours) for changes in concentrations of monosilicic acid,
19 [SiO₂(aq)], using the spectrophotometric molybdate yellow method (Greenberg et al., 1985).

20

1 **2.2 Small angle X-ray scattering (SAXS) procedure**

2 All SAXS measurements were carried out at station 6.2m at the Synchrotron Radiation Source (SRS),
3 Daresbury Laboratory, UK. The parameters that affected the data collection are summarized below and all
4 details about the configuration for station 6.2m can be found in Cernik et al. (2004).

5 A wavelength of 1.4 Å and a sample-to-detector distance of 3.75 m were used. Data were collected with a
6 60° quadrant one-dimensional small-angle detector (gas microgap, multi-wire; Berry et al. 2003; Helsby
7 et al. 2003) and a pair of ion chambers (positioned pre- and post-sample) that monitored the incoming and
8 transmitted beam intensities, respectively. The q-axis was calibrated with the scattering pattern of wet rat-
9 tail collagen.

10 Time-resolved SAXS spectra were collected every 5 minutes over 3 hours. Due to beam line settings and
11 experimental system operating procedures the first scattering pattern could only be acquired 10 minutes
12 after the cell was filled with solution (i.e., ~ 5 min to fill cell, to start SAXS experiments and to secure the
13 hutch; 5 min to acquire the first data point). Data reduction (i.e., correction for detector alinearities,
14 decaying ion beam – using the post-sample ion chamber values, and background scattering) of the 1-D
15 SAXS data was carried out using the program XOTOKO (SRS software packages, Daresbury). The
16 reduced data was further analyzed using GNOM, an indirect transform program for SAXS data
17 processing (Svergun, 1992), to derive information about the size and polydispersity of the growing
18 particles. In the case of a dilute, monodisperse system, GNOM provides an estimate for the radius of
19 gyration, R_g (a shape independent radius) and evaluates a distance distribution function, $p(R_g)$. For
20 spherical particles, $p(R_g)$ is usually Gaussian shaped (Svergun and Koch, 2003) and R_g is given by the
21 apex of the $p(R_g)$ curve.

22

1 **2.3 Dynamic light scattering (DLS)**

2 The DLS experiments were also carried out in situ and in a time resolved manner. Data was collected
3 with a Zetasizer Nano ZS (Malvern Instruments) equipped with a He–Ne laser [$\lambda = 633 \text{ nm}$], and a
4 backscatter detector at a fixed angle of 173° . These settings permit the real-time recording of an intensity
5 autocorrelation function, which is transformed into volume functions to obtain particle size information.
6 In contrast to SAXS, where all experiments were carried out at 30°C , we also used the heating capability
7 of the DLS instruments in order to monitor particle growth (i.e., hydrodynamic particle diameter and
8 polydispersity) also as a function of final temperature, i.e., at 30, 40, 50 and 60°C .

9

10 **2.4 Electron Microscopy**

11 Silica nanoparticles were imaged either with a field-emission gun scanning electron microscope (FEG-
12 SEM) or a transmission electron microscope (TEM). For FEG–SEM, a few millilitres of a polymerising
13 solution were filtered at specific time intervals through $0.1 \mu\text{m}$ polycarbonate filters. These were
14 immediately washed with distilled water and left to dry at ambient temperatures. The filter papers were
15 coated with 3 nm platinum and imaged with a LEO 1530 FEG–SEM using a working distance of 3 mm
16 and a beam intensity of 3 kV. TEM samples were prepared by depositing a droplet of the reacting
17 solutions on formvar coated copper grids. The grids were air-dried and imaged using a Philips CM10
18 TEM at an accelerating voltage of 80 kV.

19

1 2.5 Particle size and kinetic analysis

2 The change in radius of the resulting particles was evaluated from the radius of gyration, R_g , which is a
3 shape independent radius and is derived from the SAXS data using the computer code GNOM (Svergun,
4 1992) through a whole pattern fitting algorithm. The obtained R_g values were normalised:

$$5 \quad \alpha = \left(\frac{R_{g_t}}{R_{g^{\max}}} \right)^3 \quad (\text{Eqn. 1})$$

6 where R_{g_t} is R_g at a given time t , and $R_{g^{\max}}$ is R_g at the end of the reaction. Based on our previous work
7 (Tobler et al., 2009) we know that the forming silica nanoparticles are spherical in shape and thus the real
8 particle radius, R , is calculated via (Guinier, 1939):

$$9 \quad R_g^2 = \frac{3}{5} R^2 \quad (\text{Eqn. 2})$$

10 The kinetic parameters for the nucleation and growth of the silica nanoparticles (i.e., reaction mechanism,
11 reaction order and rate constant, critical nuclei size) were evaluated from the time-resolved SAXS data
12 using the Chronomal (CM) kinetic model (Nielsen, 1964; Tobler et al., 2009). Full theoretical details
13 about this kinetic model and the specifics about SAXS data analysis are given in Tobler et al. (2009).
14 Briefly, the Chronomal kinetic model is a population-dynamics based kinetic model, which is used in two
15 stages. In a first stage, the experimentally obtained growth profiles (R_g vs. time; obtained from GNOM)
16 are converted and normalised to give the degree of reaction, α , ($0 < \alpha \leq 1$ with $\alpha = 0$ meaning no
17 scattering above background and $\alpha = 1$ denoting the end of the reaction or no more change in scattering
18 intensity). In a second step, 3 different types of reaction mechanisms (chemical, surface, or diffusion
19 controlled) and varying reaction orders are fitted to the normalised reaction profiles in order to obtain the
20 best fit (i.e., highest regression coefficient, R_r^2). From these fits, the critical nuclei radii, R_0 , (by
21 extrapolating to $t = 0$), and the reaction rate constants, k are derived (Tobler et al., 2009).

3. RESULTS AND DISCUSSION

We quantified the kinetics and mechanisms of silica polymerisation and nucleation and growth of silica nanoparticles in situ and in a time resolved manner with the polymerisation being induced by the rapid cooling of a supersaturated silica solution. This way we mimicked silica sinter formation processes in natural geothermal hot springs through experiments conducted with solutions with varying silica concentrations (640 vs. 960 ppm SiO₂), ionic strengths (0.03 vs. 0.06 IS) and final temperatures (30 to 60°C). These conditions are often the dominant conditions leading to silica sinter formation in major geothermal areas in Iceland or New Zealand (e.g., Mountain et al., 2003; Tobler et al 2008 and references therein).

3.1 Silica polymerisation: [SiO₂(aq)] over time

In Figure 2A, the time dependent decrease in monosilicic acid concentrations, [SiO₂(aq)], as a function of initial silica concentration (640 and 960ppm SiO₂) and ionic strength (0.03 and 0.06 IS) is shown. The plot reveals that the initial silica concentration and thus the degree of silica supersaturation had a major impact on the rate of silica polymerisation in that the depletion of [SiO₂(aq)] in the 960ppm SiO₂ experiment is markedly faster compared to the polymerisation in the experiment at lower initial silica concentration (640ppm, Fig. 2A). Starting from 960ppm ~ 75% of the monosilicic acid polymerised within the first 20 minutes (with respect to amorphous silica solubility at 30°C; dotted line in Fig. 2A), whereas only 28% polymerised in the 640 ppm experiment. In contrast, ionic strength had little to no effect on the overall decrease of [SiO₂(aq)] over time. Note that after 2 hours, all three data sets levelled off, approaching a monosilicic acid concentration close to the amorphous silica solubility at 30°C (Fig. 2A).

1 The effect of temperature (30 to 60°C) on the polymerisation process for solutions with 960ppm SiO₂ and
2 IS=0.03 (Figure 2B) showed that again within the first 20 minutes, and regardless of final temperature,
3 approximately 80% of the initial [SiO₂(aq)] polymerised, reaching ~ 360 - 400 ppm. Thereafter, the
4 polymerisation process proceeded considerably slower. When comparing the 30°C and 60°C profiles,
5 polymerisation occurred, as expected, faster at 30°C (dotted lines in Fig. 2B).

6

7 **3.2 Silica nanoparticle growth: SAXS**

8 The typical time-resolved change in the SAXS patterns during an in situ experiment (Figure 3) revealed
9 that with increasing time the total scattering intensity, $I(q)$, and the slope at low q of the scattering curve
10 increased. An increase in $I(q)$ indicates an increase in electron density contrast between matrix and the
11 newly formed particles but also an increase in total scattering volume (i.e., increase in particle volume or
12 number). The increase in slope at low q (Guinier region, $qR_g < 1$; Guinier, 1939) indicates an increase in
13 particle size with time.

14 From the GNOM analyses of the patterns, and applying equation [2], the growth of the particle radius, R ,
15 as a function of time at different silica concentrations and ionic strengths was evaluated (Figure 4A).
16 Comparing growth profiles at high [SiO₂] (960ppm) but at different IS (0.03 vs. 0.06) showed an identical
17 behaviour with time. The first scattering pattern (10 minutes) revealed particles with a radius of ~ 1.5 nm
18 and over the three hours of the experiment the radius increased and reached a plateau at approximately 3.5
19 nm. In contrast, particle growth was significantly delayed in the experiment at lower [SiO₂] (640ppm,
20 0.06 IS; Fig. 4A crosses), and particles were only observed after an induction period of ~ 60 minutes.
21 Again, the first particles had a radius of approximately 1.5 nm, and this steadily increased in size, but in
22 this experiment, even after 3 hours a plateau in the growth profile and thus a stable particle size was not
23 reached. Extrapolation of the growth curve to a plateau suggested that the time to reach the end of particle

1 growth at this concentration was significantly longer (possibly up to 6 hours, Fig. 4A). Note that particles
2 might have already nucleated after 15 minutes (once polymerisation started; Fig. 2) but these particles
3 may have been unstable within the polymerising solution and re-dissolved again. Possibly, particles
4 growth was induced only after a certain degree of polymerisation was reached. Furthermore, the SAXS
5 experimental and beam line configuration and the small difference between background and the first
6 scattering pattern (signal to noise issues) might have limited our data quality to evaluations that showed
7 particles with radii ≥ 1.5 nm. Thus, it is likely that using this approach and set-up we were not able to
8 detect particles with diameters < 3 nm, and hence nucleation of critical nuclei. Overall, our SAXS results
9 agreed with the profiles of the depletion in monosilicic acid concentrations over time (Fig. 2A) and
10 reaffirmed that the initial $[\text{SiO}_2]$ (i.e., silica supersaturation) was the prime control for the rate of silica
11 polymerisation and nanoparticle growth, while the differences in IS did not cause detectable deviations.

12 The second parameter evaluated with GNOM was the distance distribution function, $p(R)$, for the
13 polymerisation reaction (Figure 4B), using equation [2] to convert the R_g to R . The increase in both the
14 area under the curve and the apex of the curve indicated an increase in particle size. Importantly, the near-
15 Gaussian shape of the $p(R)$ suggested fairly monodisperse and spherical silica nanoparticles. The
16 observed slight skew to the right and the tails at higher R , is related to the presence of some aggregates or
17 a certain degree of polydispersity. Note that the shape and evolution of the $p(R)$ curves did not differ
18 between experiments (i.e., over the studied SiO_2 / IS) and all $p(R)$ plots were slightly skewed towards the
19 right.

20

21 **3.3 Silica nanoparticle growth: DLS**

22 The time-resolved DLS data shows the time-dependent change in the scattering of laser light caused by
23 the Brownian motion of the forming silica particles which is related to changes in the apparent mean

1 hydrodynamic diameter of the growing particles (Fig. 5). The large scatter in the data with the particle
2 diameter errors reaching 36% is due to the low resolution of DLS at small particle sizes (Fig. 5; as
3 compared to the 1 - 3% error for the SAXS data). Nevertheless, the particle growth rate vs. $[\text{SiO}_2]$ / IS
4 trends are comparable to those observed with SAXS (Fig 4). Starting with 960ppm SiO_2 resulted in silica
5 nanoparticles with a hydrodynamic diameter of approximately 3 nm shortly after the measurements were
6 initiated (16 min). This diameter matched perfectly with the 1.5 nm radius derived from the first SAXS
7 pattern (10 min, Fig 4A). In contrast, at lower $[\text{SiO}_2]$ (640ppm, Fig. 5A), it took only ~ 40 minutes for the
8 first DLS patterns to reveal scatter above background. Despite the far larger errors of DLS compared to
9 SAXS, this is a ~ 20 minutes shorter induction time compared to the SAXS results (Fig 4A).

10 When the DLS measurements were carried out at various final temperatures (30 - 60°C) the data revealed
11 no detectable effect on particle size or growth rate (Figure 5B). In all growth profiles, the first detectable
12 particles had a diameter of around 3 nm which then increased to about 5 ± 1 nm within the first 90
13 minutes. The silica solubility at 60°C is higher compared to 30°C and this would suggest a lower growth
14 rate, i.e., slower polymerisation rates at higher temperatures. However, the larger errors of the DLS
15 measurements make a further evaluation of absolute differences impractical.

16 Taken together, the SAXS and DLS results both confirmed our previous study that showed that the rate of
17 silica polymerisation and nanoparticle formation was affected by increasing silica concentration (Tobler
18 et al., 2009; supersaturation reached at 25°C and through a pH drop). Our previous results further
19 demonstrated that a change in ionic strength affected the silica solubility and thus the polymerisation
20 reaction and particle growth rate. However, in the current study (where supersaturation was reached by a
21 fast temperature drop from 230°C) the variations in tested IS (0.03 vs. 0.06) as well as T (30 to 60°C)
22 showed no effect on nanoparticle formation or the differences could not be resolved with the techniques
23 applied in this study.

24

1 **3.4 Silica nanoparticle imaging / size analysis: electron microscopy**

2 The particle sizes obtained from SAXS and DLS were verified by imaging of the resulting particles at
3 various time steps. After 3 hours of polymerisation in a solution with 960ppm SiO₂ and IS = 0.03 tiny but
4 rounded particles and particle aggregates (Fig. 6A) were observed. Although a rough particle size could
5 be derived, the FEG-SEM resolution was too low to obtain accurate measurements. A more accurate
6 particle size value was derived from TEM photomicrographs (Fig. 6B) where the individual particles
7 confirmed the spherical shape and fairly monodisperse size distribution observed with SAXS. The
8 average particle diameters and the polydispersity (i.e., standard deviation) was determined from samples
9 quenched and imaged at two aging times (2 and 3 hours) and results are listed in the table of Figure 6
10 along with SAXS and DLS data for comparison. The data revealed that the sizes derived from the TEM
11 images were significantly smaller (up to 50%) than those derived from DLS and SAXS. This was not
12 unexpected as for TEM analyses samples were dried and placed under high vacuum and thus the
13 amorphous silica nanoparticles underwent dehydration and relaxation. This caused the highly hydrous and
14 open-structured particles to collapse and aggregate as compared to SAXS and DLS where silica
15 nanoparticles were examined in their native / hydrated state (Tobler et al., 2009).

16

17 **3.5 Reaction kinetics of silica nanoparticle formation**

18 In all experiments, the reacting solutions were supersaturated with respect to amorphous silica and
19 particle nucleation was assumed to be homogeneous and instantaneous (Tobler et al., 2009). Upon
20 reaching the desired temperature at high [SiO₂], silica nanoparticles nucleated instantaneously as revealed
21 by the excellent fit of the normalised SAXS data to the Chronomal kinetic model (regression coefficient,
22 R_r^2 , = 0.99; Fig. 7). In contrast, at lower supersaturation (640 ppm SiO₂) both SAXS and DLS results
23 revealed that nucleation was preceded by an induction period, and thus at lower silica concentration

1 nucleation was not instantaneous. This was due to the delayed polymerisation reaction as shown by the
2 slower decrease in monosilicic acid concentration in Fig 2A. At this lower silica concentration even after
3 3 hours a final particle size was not reached so a fitting to the Chronomal model was not feasible.

4 From the first SAXS pattern (10 minutes after polymerisation was induced) particles with radii of ~ 1.5
5 nm were derived. At the time of our experiments beam line configurations and low signal to noise issues
6 prevented us from collecting patterns immediately after the start of the experiments and thus the first
7 measured particle radii do not represent critical nuclei sizes. Nevertheless, the critical nuclei sizes could
8 be estimated via two procedures. First, critical nuclei were estimated from the Gibbs-Kelvin equation
9 following our previous approach (Tobler et al., 2009). Under the conditions tested here, the Gibbs-Kelvin
10 critical nuclei, R_0^+ , was not affected by ionic strength but was considerably smaller in experiments that
11 started with solutions with 960ppm SiO_2 ($R_0^+ = 0.85$ nm) compared to a critical nuclei radius with $R_0^+ =$
12 1.07 nm in experiments starting with 640ppm SiO_2 . This was not unexpected as the nucleation process
13 has a higher driving force in more saturated solutions thus enabling the formation and stabilisation of
14 many but smaller nuclei (Lasaga, 1998). A second estimate of the critical nuclei radii for the 960ppm
15 SiO_2 / 0.03 IS experiment was obtained from the excellent fit between data and the Chronomal kinetic
16 model (Fig. 7). The results revealed a critical nucleus of $R_0 = 1.47$ nm which was considerably larger than
17 the R_0^+ value from the Gibbs-Kelvin approach (0.85 nm). This discrepancy is likely due to the fact that
18 the Gibbs-Kelvin approach uses a surface energy value that may be erroneous as it was not determined for
19 highly hydrated silica nanoparticles surfaces. In contrast, for Chronomal analyses, the full scattering
20 pattern was fitted and the extrapolation to time 0 is more representative for the true critical radius.
21 Furthermore, the fact that the Gibbs-Kelvin approach accounts solely for the degree of supersaturation,
22 but does not consider other parameters (e.g., induction time, presence of salts etc) also influences the
23 critical nuclei size evaluation.

24

1 The nucleation stage was followed by the fast decrease of monosilicic acid (Fig. 2) and the 3-dimensional
2 growth of silica nanoparticles (Fig. 4A). The spherical shape of the silica particles was verified by SEM
3 and TEM (Fig. 6) and also by the good fit of the SAXS data to the Chronomal model (which assumes 3-
4 D, classical growth, Fig. 7). The Chronomal analyses further showed that particle growth obeyed a first
5 order rate law with a surface-controlled mechanism which matches our previous results where silica
6 polymerisation and silica nanoparticle formation was induced through a drastic pH change. In contrast to
7 several previous studies, where Ostwald ripening and particle aggregation has been suggested as being the
8 dominant process in the later stages of silica nanoparticle formation (e.g., Iler, 1979; Perry and Keeling-
9 Tucker, 2000; Tobler et al., 2009), in the experiments discussed here the DLS measurements clearly
10 showed that aggregation did not occur. DLS is highly susceptible to the presence of even a small
11 proportion of large aggregates (i.e., 1-2% by volume; see Tobler et al., 2009). Nevertheless, the fact that
12 in the current experiments, where silica polymerisation was induced by a temperature drop, no
13 aggregation was observed, is most likely a consequence of the slower particle growth (as confirmed by
14 the SAXS data, Fig. 4A) and thus a delay of the invariable later aggregation that ultimately in natural
15 geothermal systems leads to the formation of silica sinters.

16

17 **3.6 How do silica nanoparticles form in natural settings: T- vs pH-induced process**

18 The prime aim of this study was to quantify the kinetics and mechanisms of the nucleation and growth of
19 silica nanoparticles under conditions that mimic primarily processes in natural geothermal systems – i.e.,
20 by a drastic change in temperature upon emergence of the fluids at the Earth's surface. Furthermore, we
21 wanted to show how a combination of in situ and time resolved scattering measurements can be used to
22 derive highly accurate data sets pertinent to silica particle nucleation, data sets that could be compared to
23 the vast majority of previous experiments that quantified silica nanoparticle growth through a less realistic
24 dramatic pH drop method (e.g., Alexander et al., 1954; Iler, 1979; Tobler et al., 2009 and references

1 therein). The “pH-induced” method has been so far the most practical in terms of experimental
2 approaches, but it is however, not representative of the processes occurring in natural geothermal systems,
3 where the polymerisation reaction is a result of rapid cooling of supersaturated, most often near-neutral,
4 high temperature fluids (“T – induced”). Naturally, assuming identical composition, one would expect the
5 polymerisation reaction and thus silica nanoparticle growth to be similar, regardless of the induction
6 process. The few previous studies that focused on silica polymerisation and precipitation in natural
7 geothermal waters and / or simulated natural geothermal processes (e.g., Rothbaum and Rhode, 1979;
8 Weres, 1981; Carroll et al., 1998) had demonstrated that silica polymerisation is delayed when
9 polymerisation is induced by fast cooling (compared to pH – induced). However, these studies did not
10 provide a means to determine silica nanoparticle nucleation rates and mechanism. In our previous study
11 (Tobler et al., 2009) we have however, quantified the formation of silica nanoparticles using pH-induced
12 method while applying the same set of techniques and similar solution chemistries as in the current study.
13 With the current new data set we are now in the position to compare silica polymerisation and silica
14 nanoparticle formation using equivalent solution compositions but from a ‘T-induced’ (current study) and
15 a ‘pH-induced’ (Tobler et al., 2009) approach. This way we can assess if mode of induction of silica
16 polymerisation is affecting the mechanisms and/or kinetics of silica polymerisation and nanoparticle
17 formation (T- vs. pH – induced). This comparison is summarised in Figure 8 and Table 1 and discussed
18 below.

19 The dominant trend observed in Figure 8 shows that the polymerisation and particle growth proceeded
20 faster when the reaction was induced by a change in pH (rate constant > 50% larger, Table 1). This is
21 visible through the instantaneous decrease in $[\text{SiO}_2(\text{aq})]$ and the simultaneous increase in particle size in
22 the pH-induced experiment, compared to the considerably delayed polymerisation and particle growth in
23 the T - induced experiment (Fig. 8). Furthermore, in the pH-induced experiments (Tobler et al., 2009) we
24 had observed particle aggregation while in the T-induced experiments in the current study no particle
25 aggregation was observed. Nevertheless, the important observation is that the growth mechanism is not

1 affected by the mode of achieving supersaturation and both pH- and T-induced polymerisation lead to a
2 1st order, surface-controlled growth of the silica nanoparticles.

3 Connected to the differences in reaction rates, the two different approaches also affected the critical nuclei
4 size of the forming particles. The Chronomal R_0 value was significantly smaller in the pH-induced (1.09
5 nm) compared to the T-induced experiment (>1.47 nm). Although in the T-induced experiments the
6 critical nucleus value was obtained from the high $[\text{SiO}_2]$ (960ppm) experiment, at 640ppm $[\text{SiO}_2]$,
7 however, a larger critical nucleus would be expected. This difference indicated that the critical nuclei size
8 is not solely controlled by the degree of supersaturation. This also explained the discrepancy in critical
9 nuclei size between values determined with the Gibbs-Kelvin approach and with the Chronomal model in
10 this study (see section 3.6). The Gibbs-Kelvin critical nuclei size is only dependent on the degree of
11 supersaturation and does not account for the rate at which supersaturation is established. The
12 extrapolation of the growth curve to time zero (using the Chronomal model) therefore provided a more
13 accurate estimate of the critical nuclei size.

14 The > 50 % slower rates of silica polymerisation and particle growth and the larger critical nuclei size in
15 current T-induced experiments is explained by the differences in time to establish supersaturation. In the
16 pH-induced experiments, the sudden change in pH from 12 to 7 (<30 s) induced instantaneous
17 supersaturation and thus forced the monosilicic acid to polymerise. In contrast, the cooling process of the
18 hot fluids (emerging from the high-T oven) from 230°C to 30°C took 2 to 3 minutes. This led to a more
19 gradual increase in supersaturation (as T decreased) and thus slower rates of silica polymerisation. In
20 addition, the pH- and T-dependency of silica solubility differ substantially. With regards to pH, silica
21 solubility is at a minimum around pH 6 to 9 but then increases drastically at pH > 9 (Alexander et al.,
22 1954). In the case of temperature, the solubility does not exhibit any dramatic changes but steadily
23 increases with increasing T (Gunnarsson and Arnorsson, 2000). Thus the radical change in pH imposed a
24 faster attainment of supersaturated conditions and thus the polymerisation reaction was substantially

1 faster compared to the polymerisation induced by the gradual change in T, which also explains the
2 differences in reaction rates and critical nuclei sizes.

3 Results from this study are critical to the understanding of a variety of natural processes. For example,
4 microbial silicification and fossilisation have been widely investigated in laboratory studies to determine
5 the geochemical conditions for optimal microbial preservation in ancient and modern silica sinters (e.g.,
6 Benning et al 2004a,b; Yee et al., 2003; Lalonde et al., 2005 and references therein). In most of these
7 experiments, silica polymerisation and precipitation were induced by a change in pH. Therefore it is
8 likely that the reported optimal silicification conditions may need to be reconsidered in light of the new
9 results presented here. Moreover, energetic considerations and geochemical modelling of other processes
10 that involve silica nanoparticles formation from cooling supersaturated waters (e.g., sinter formation,
11 silica diagenesis) need to be adjusted to account for lower polymerisation and precipitation rates shown in
12 this study. However, comparisons with natural silicification and sinter growth experiments carried out in
13 modern active geothermal pools (i.e., Mountain et al 2003, Tobler et al 2008) showed that silica
14 precipitation and microbial silicification is highly dependent on supersaturation and polymerisation rates
15 but that in natural settings salt content and the organic compounds of microbial systems also highly affect
16 silicification rates.

17 The kinetics of the nucleation, growth and aggregation of silica nanoparticles in cooling waters have also
18 direct implication for industrial processes. For example, silica precipitation and scaling at geothermal
19 power plants is a well known problem. Accurate knowledge of rates of silica polymerisation and silica
20 nanoparticle formation in cooling silica supersaturated waters is thus critical to predict the level of silica
21 scaling that can be expected in cooling geothermal waters. Equally, this data can help to optimise
22 handling strategies for the fast cooling geothermal water to reduce silica scaling in key positions such as
23 pipelines and injection wells.

1 Importantly, however, this study also showed that our newly developed high-temperature system run in-
2 line with time resolved aqueous analyses and in situ and time resolved particle formation and these
3 particle property measurements have now lead to an accurate picture of a nucleation and growth process
4 of silica nanoparticles. These results are highly relevant to our understanding of modern and ancient silica
5 sinter formation processes both on Earth and potentially elsewhere.

6

7

ACKNOWLEDGEMENTS

8 The authors thank Christopher Martin for beamtime and technical assistance to carry out SAXS
9 measurements at station 6.2m at the Synchrotron Radiation Source (SRS), Daresbury Laboratory, UK.
10 Financial support via a PhD fellowship for DJT from the Earth and Biosphere Institute (University of
11 Leeds, UK), and research funds for LGB from the University of Leeds are acknowledged.

12

13

REFERENCES

- 14 Alexander G. B., Heston W. M. and Iler R. K. (1954) The solubility of amorphous silica in water. *J. Phys.*
15 *Chem.* **58**, 453-455.
- 16 Benning L. G., Phoenix V. R., Yee N., and Konhauser K. O. (2004a) The dynamics of cyanobacterial
17 silicification: An infrared micro-spectroscopic investigation. *Geochim. Cosmochim. Acta* **68**, 729–
18 741.
- 19 Benning L. G., Phoenix V. R., Yee N. and Tobin M.J. (2004b) Molecular characterization of
20 cyanobacterial silicification using synchrotron infrared micro-spectroscopy. *Geochim. Cosmochim.*
21 *Acta* **68**, 743–757.

- 1 Benning L. G. and Mountain B. M. (2004) The silicification of microorganisms: a comparison between in
2 situ experiments in the field and laboratory. In *Water-Rock Interaction* (eds. Wanty and Seal II).
3 Taylor and Francis Group, London. pp. 3-10.
- 4 Berry A., Helsby W. I., Parker B. T., Hall C. J., Buksh P. A., Hill A., Clague N., Hillon M., Corbett G.,
5 Clifford P., Tidbury A., Lewis R. A., Cernik B. J., Barnes P. and Derbyshire G. E. (2003) The
6 RAPIP2 x-ray detection system. *Nucl. Instrum. Meth. A* **513**, 260-263.
- 7 Carroll S., Mroczek E., Alai M. and Ebert M. (1998) Amorphous silica precipitation (60 to 120 degrees
8 C): Comparison of laboratory and field rates. *Geochim. Cosmochim. Acta* **62**, 1379–1396.
- 9 Cernik R. J., Barnes P., Bushnell-Wye G., Dent A. J., Diakun G. P., Flaherty J. V., Greaves G. N., Heeley
10 E. L., Helsby W., Jaques S. D. M., Kay J., Rayment T., Ryan A., Tang C. C. and Terrill N. J.
11 (2004) The new materials processing beamline at the SRS Daresbury, MPW6.2. *J. Synchrotron*
12 *Radiat.* **11**, 163-170.
- 13 Conrad C. F., Yasuhara H., Bandstra J. Z., Icopini G. A., Brantley S. L. and Heaney P. J. (2007)
14 Modeling the kinetics of silica nanocolloid formation and growth in aqueous solutions as a function
15 of pH and ionic strength. *Geochim. Cosmochim. Acta* **71**, 531-542.
- 16 Guinier A. (1939) La diffraction des rayons X aux tres petits angles: application al'étude de phenomenes
17 Ultramicroscopiques. *Ann. Phys.* **12**, 161-237.
- 18 Gunnarsson I. and Arnórsson S. (2000) Amorphous silica solubility and the thermodynamic properties of
19 H_4SiO_4 in the range of 0° to 350°C at P_{sat} . *Geochim. Cosmochim. Acta* **64**, 2295-2307.
- 20 Greenberg A. E., Trussell R. R. and Clesceri L. (1985) *Standard Methods for the Examination of Water*
21 *and Wastewater*. American Public Health Association, New York, 209 pp.
- 22 Helsby W. I., Berry A., Buksh P. A, Hall C. J. and Lewis R. A. (2003) The RAPID2 interpolating system.
23 *Nucl. Instrum. Meth. A* **510**, 138-144.
- 24 Halasz I., Kierys A., Goworek J., Liu H. M. and Patterson R. E. (2011) (^{29}Si) NMR and Raman Glimpses
25 into the Molecular Structures of Acid and Base Set Silica Gels Obtained from TEOS and Na-
26 Silicate. *J. Phys. Chem. C* **115**, 24788 – 24799.
- 27 Handley K. M., Campbell K. A., Mountain B. W. and Browne P. R. L. (2005) Abiotic–biotic controls on
28 the origin and development of spicular sinter: in situ growth experiments, Champagne Pool,
29 Waiotapu, New Zealand. *Geobiol.* **3**, 93–114.

- 1 Iler R. K. (1979) *The chemistry of silica*, John Wiley, New York.
- 2 Konhauser K. O., Phoenix V. R., Bottrell S. H., Adams D. G. and Head I. M. (2001) Microbial–silica
3 interactions in Icelandic hot springs sinter: possible analogues for some Precambrian siliceous
4 stromatolites. *Sedimentology* **48**, 415–433.
- 5 Lalonde S. V., Konhauser K. O., Reysenbach A. L. and Ferris F. G. (2005) The experimental silicification
6 of Aquificales and their role in hot spring formation. *Geobiology* **3**, 41–52.
- 7 Lasaga A. C. (1998) *Kinetic Theory in the Earth Sciences*. Princeton University Press, Princeton, New
8 Jersey, 811 p.
- 9 Makrides A. C., Turner M. and Slaughter J. (1980) Condensation of silica from supersaturated silicic acid
10 solutions. *J. Colloid Interface Sci.* **73**, 345–367.
- 11 Mountain B. W., Benning L. G. and Boerema J. (2003) Experimental studies on New Zealand hot spring
12 sinters: rates of growth and textural development. *Can. J. Earth Sci.* **40**, 1643–1667.
- 13 Nielsen A. E. (1964) Kinetics of precipitation. In *International Series of Monographs on Analytical*
14 *Chemistry* (eds. R. Belcher and L. Gordon). Pergamon Press, Oxford, UK.
- 15 Pabisch S., Feichtenschlager B., Kickelbick G. and Peterlik H. (2012) Effect of interparticle interactions
16 on size determination of zirconia and silica based systems – A comparison of SAXS, DLS, BET,
17 XRD and TEM. *Chem. Phys. Lett.* **521**, 91–97.
- 18 Perry C. C. and Keeling-Tucker T. (2000) Biosilicification: the role of the organic matrix structure
19 control. *J. Biol. Inorg. Chem.* **5**, 537–550.
- 20 Rimstidt J. D. and Barnes H. L. (1980) The kinetics of silica-water reactions. *Geochim. Cosmochim. Acta*
21 **44**, 1683–1699.
- 22 Rothbaum H. P. and Rhode A. G. (1979) Kinetics of silica polymerisation and deposition from dilute
23 solutions between 5 and 180°C. *J. Colloid Interface Sci.* **71**, 533–559.
- 24 Stöber W., Fink A. and Bohn E. (1968) Controlled growth of monodisperse silica spheres in the micron
25 size range. *J. Colloid Interface Sci.* **26**, 62–69.
- 26 Svergun D. I. (1992) Determination of the regularization parameter in indirect-transform methods using
27 perceptual criteria. *J. Appl. Cryst.* **25**, 495–503.

- 1 Svergun D. I. and Koch M. H. J. (2003) Small-angle scattering studies of biological macromolecules in
2 solution. *Rep. Prog. Phys.* **66**, 1735–1782.
- 3 Tobler D. J. and Benning L. G. (2011) Bacterial diversity in five Icelandic geothermal waters:
4 temperature and sinter growth rate effects. *Extremophiles* **15**, 473-485.
- 5 Tobler D. J., Stefánsson A. and Benning L. G. (2008) In-situ grown silica sinters in Icelandic geothermal
6 areas. *Geobiology* **6**, 481-502.
- 7 Tobler D. J., Shaw S. and Benning L. G. (2009) Quantification of initial steps of nucleation and growth of
8 silica nanoparticles: an in-situ SAXS and DLS study. *Geochim. Cosmochim. Acta* **73**, 5377-5393.
- 9 Weres O., Yee A. and Tsao L. (1981) Kinetics of silica polymerisation. *J. Colloid Interface Sci.* **84**, 379-
10 402.
- 11 Yee N., Phoenix V. R., Konhauser K. O., Benning L. G. and Ferris F. G. (2003) The effect of
12 cyanobacteria on Si precipitation kinetics at neutral pH: Implications for bacterial silicification in
13 geothermal hot springs. *Chem. Geol.* **199**, 83-90.

14

15

FIGURE CAPTIONS

16 Figure 1: Schematic diagram of experimental set up to simulate a natural geothermal system where silica
17 nanoparticles form via the fast cooling of a supersaturated monomeric silica solution (modified after
18 Benning and Mountain, 2004). The simulator is interlinked with the in situ and real-time scattering cells
19 and detectors.

20 Figure 2: Time-dependent decrease in monosilicic acid concentrations, $[\text{SiO}_2(\text{aq})]$, as a function of (A)
21 initial silica content (640 vs. 960 ppm SiO_2) and ionic strength (0.03 vs. 0.06 IS) and (B) final
22 temperatures (30 to 60°C) in experiment with 960 ppm SiO_2 and 0.03 IS. Dotted lines represent
23 amorphous silica solubility in solutions with IS = 0.03 (based on Gunnarsson and Arnórsson, 2000).

1 Figure 3: Log-log plot of the scattering intensity as a function of scattering angle and time (960ppm SiO₂,
2 0.03 IS, 30°C). Note that SAXS patterns were collected every 5 min (up to 3 h) but for clarity only a few
3 patterns are shown. The errors for each data point are smaller than the symbols (<3%).

4 Figure 4: A) Time course of particle radius (R, in nm) in solutions with 640ppm and 960ppm SiO₂ and
5 different IS (errors smaller than symbols; ~3%). B) Example of a pair distribution function p(R) plot for
6 the scattered silica nanoparticles as a function of radius, R, and time (960ppm SiO₂, 0.03 IS).

7 Figure 5: A) Hydrodynamic diameters of growing silica nanoparticles in solutions that had a final
8 temperature of 30°C evaluated from the DLS volume data. The arrow indicates the induction period (i.e.,
9 first detectable particle) for the 640ppm SiO₂ experiment (% errors are average values for each
10 experiment). B) DLS growth profiles for silica nanoparticles formed in a solution with 960ppm SiO₂ and
11 0.03 IS that had reached various final temperatures.

12 Figure 6: (A) FEG-SEM image (white spots = particles) and (B) TEM image (black spots = particles) of
13 silica nanoparticles grown for 3 hours in a solution with 960ppm SiO₂ and IS = 0.03. Table shows
14 comparison of particle diameters obtained from SAXS, DLS and TEM.

15 Figure 7: Reaction process, α (Eqn. 1), for the 960ppm SiO₂ / 0.03 IS experiment. The solid line
16 represents the fit to the Chronomal kinetic model from which the kinetic parameters were derived.

17 Figure 8: The effect of T- and pH - induced silica supersaturation on (A) the time-dependent depletion in
18 [SiO₂(aq)] and (B) the increase in SAXS particle radius over time in solutions with 640ppm SiO₂ (at
19 30°C). Dotted lines represent amorphous silica solubility in solutions with IS = 0.03 (from Gunnarsson
20 and Arnórsson, 2000).

21

22

1

TABLES

2 Table 1: Comparison between the derived kinetic parameters for the pH - and T - induced experiments for
 3 solutions with initial 640ppm SiO₂.

	pH – induced	T – induced
Nucleation		
R ₀ ⁺ Gibbs-Kelvin Approach	1.07	1.07
R ₀ Chronomal Analysis	1.09	> 1.47 ^a
Induction period	No	~ 60 min
Particle growth		
1st order reaction, surface-controlled	yes	yes ^b
Chronomal rate constant (x10 ⁻⁴ s ⁻¹)	3.18	<1.46 ^a
Aggregation		
DLS	yes	no

4 ^aChronomal kinetic parameters from 960 ppm SiO₂ experiment

5 ^bAssuming particle growth mechanism is not affected by SiO₂ concentration

6

7

Figure 1
[Click here to download high resolution image](#)

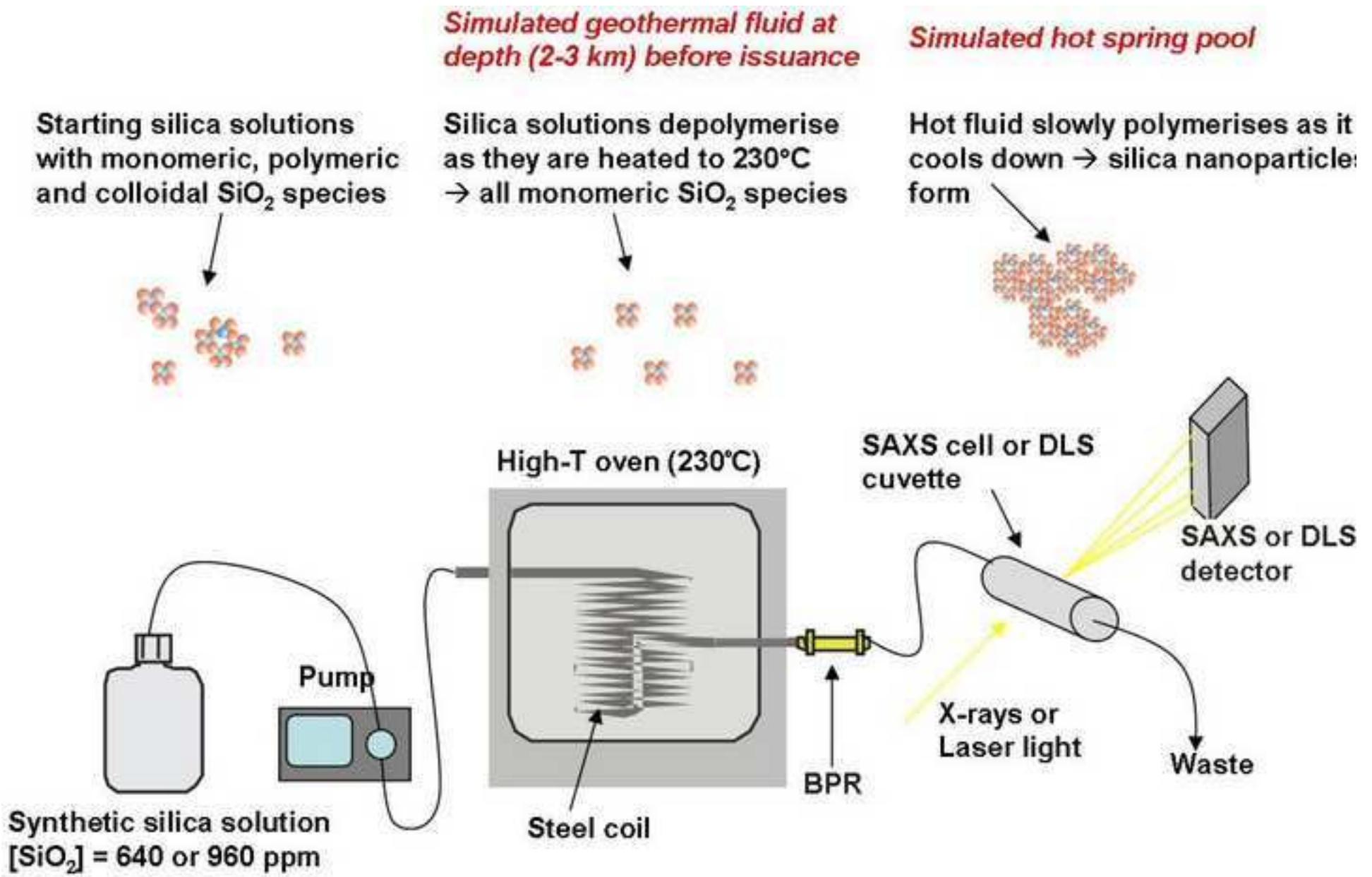


Figure 2

[Click here to download high resolution image](#)

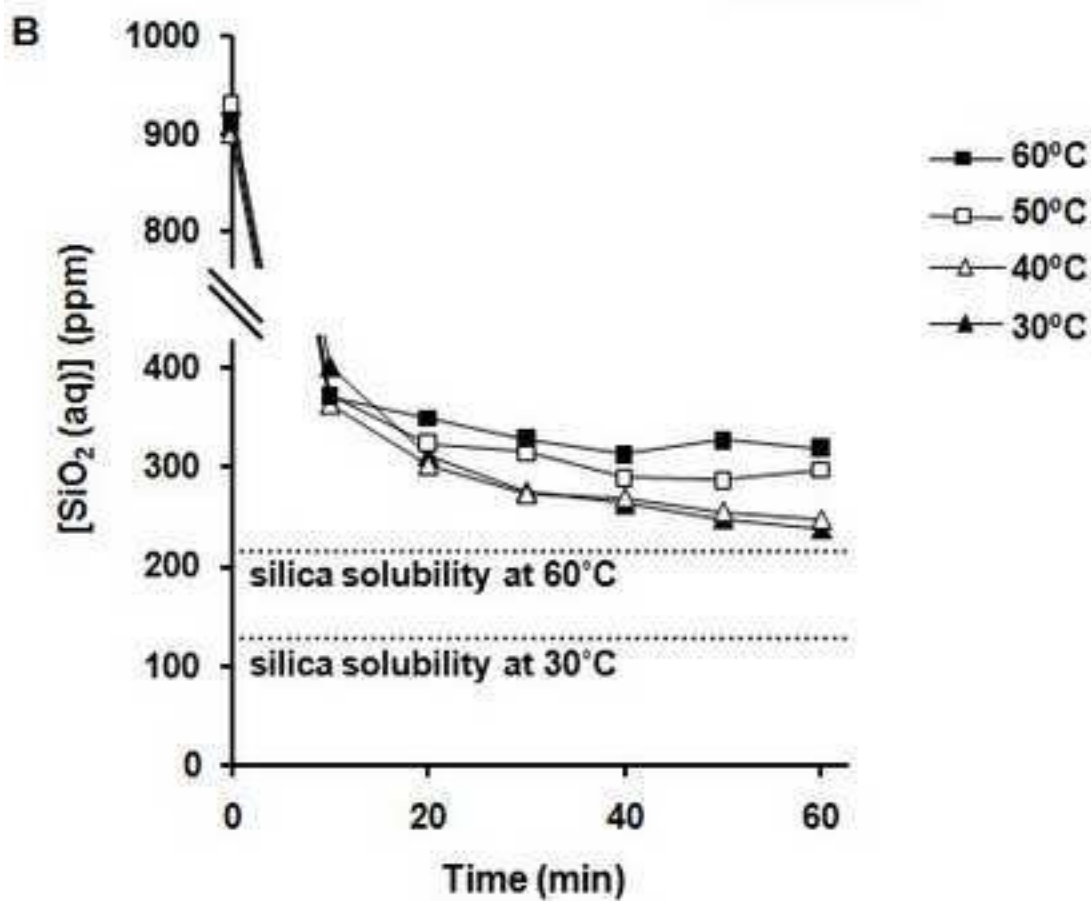
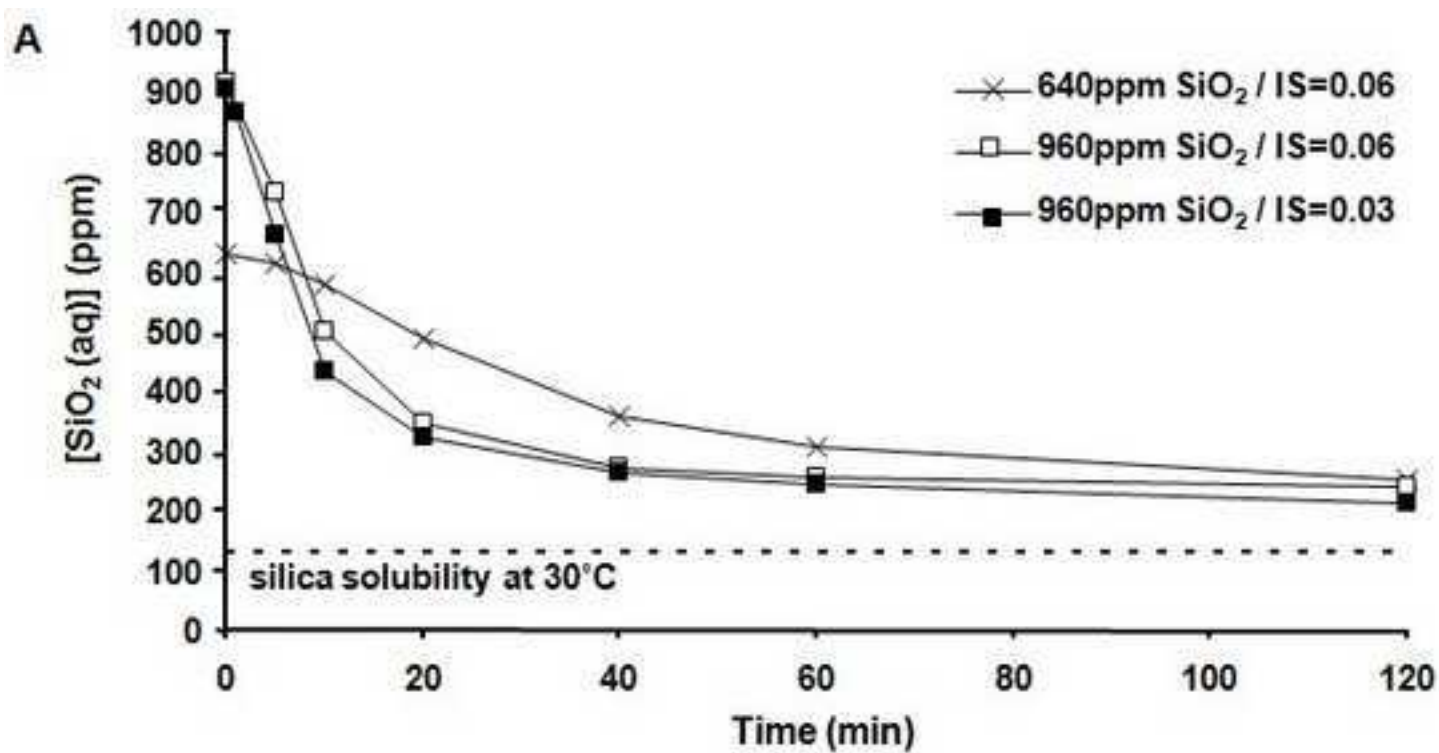


Figure 3
[Click here to download high resolution image](#)

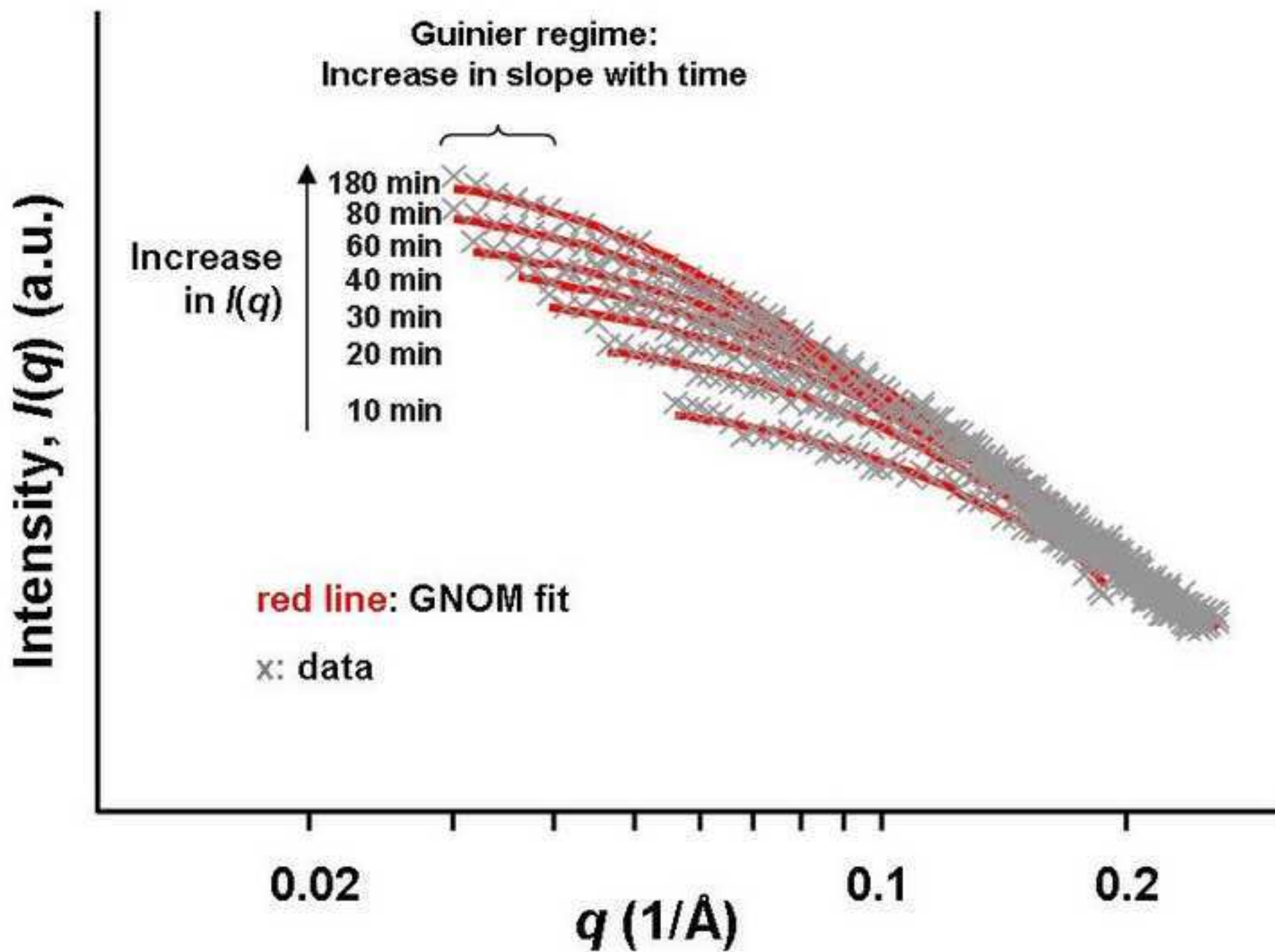


Figure 4
[Click here to download high resolution image](#)

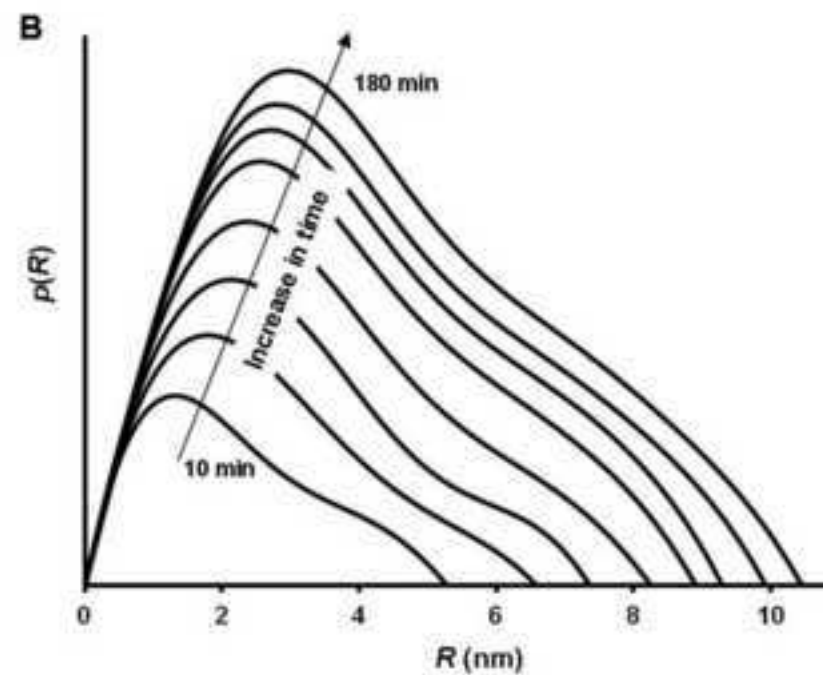
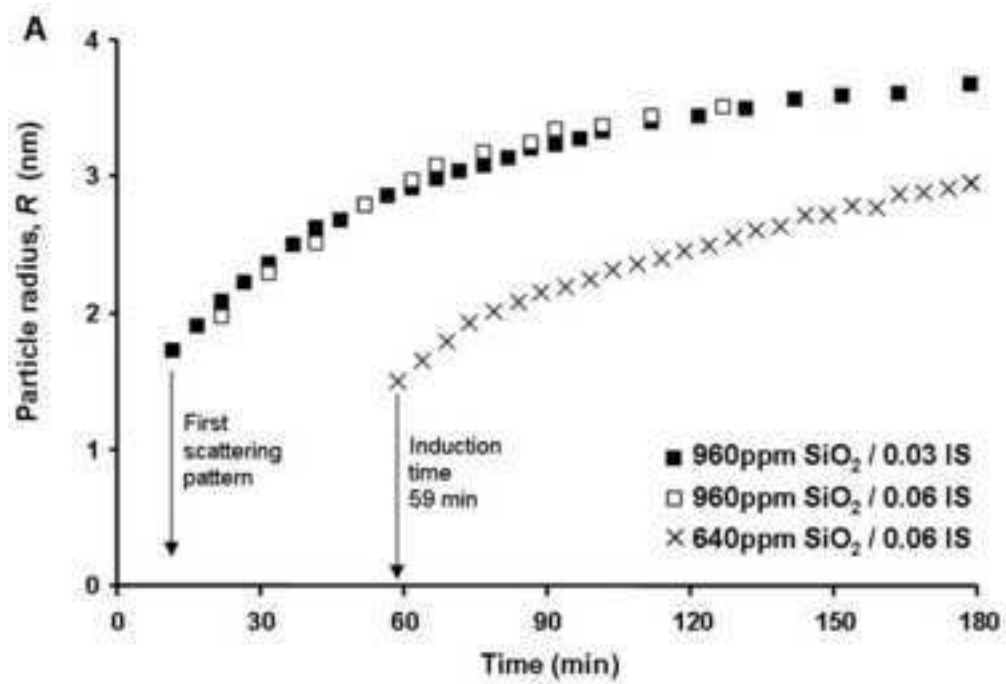


Figure 5
[Click here to download high resolution image](#)

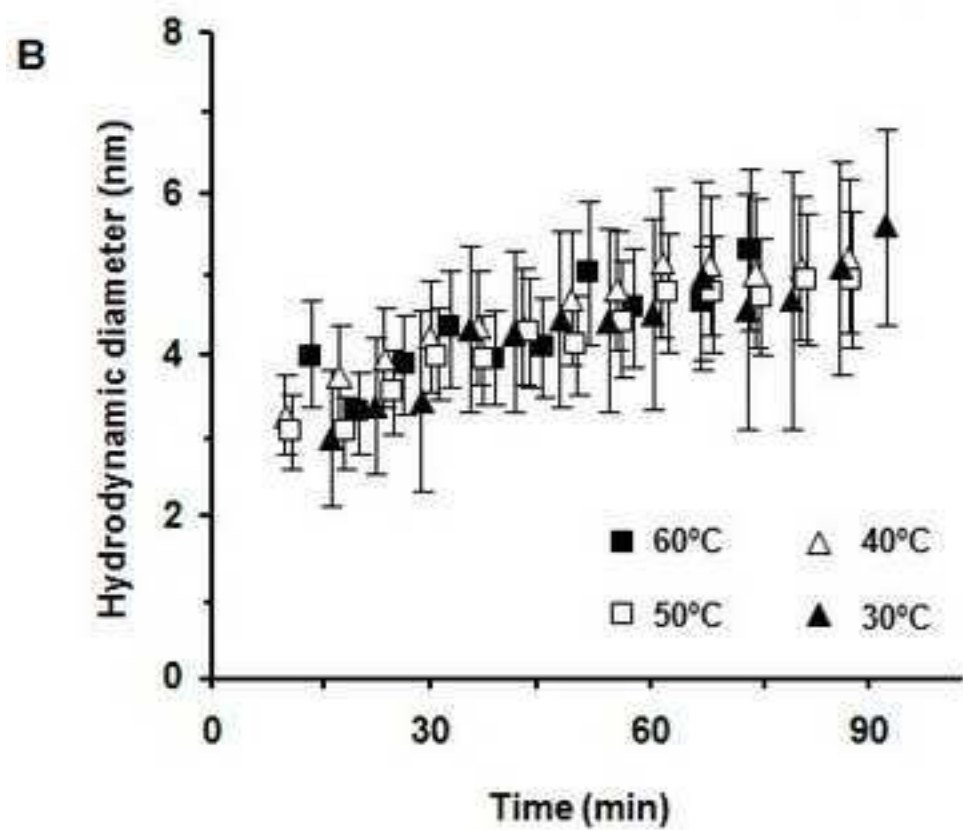
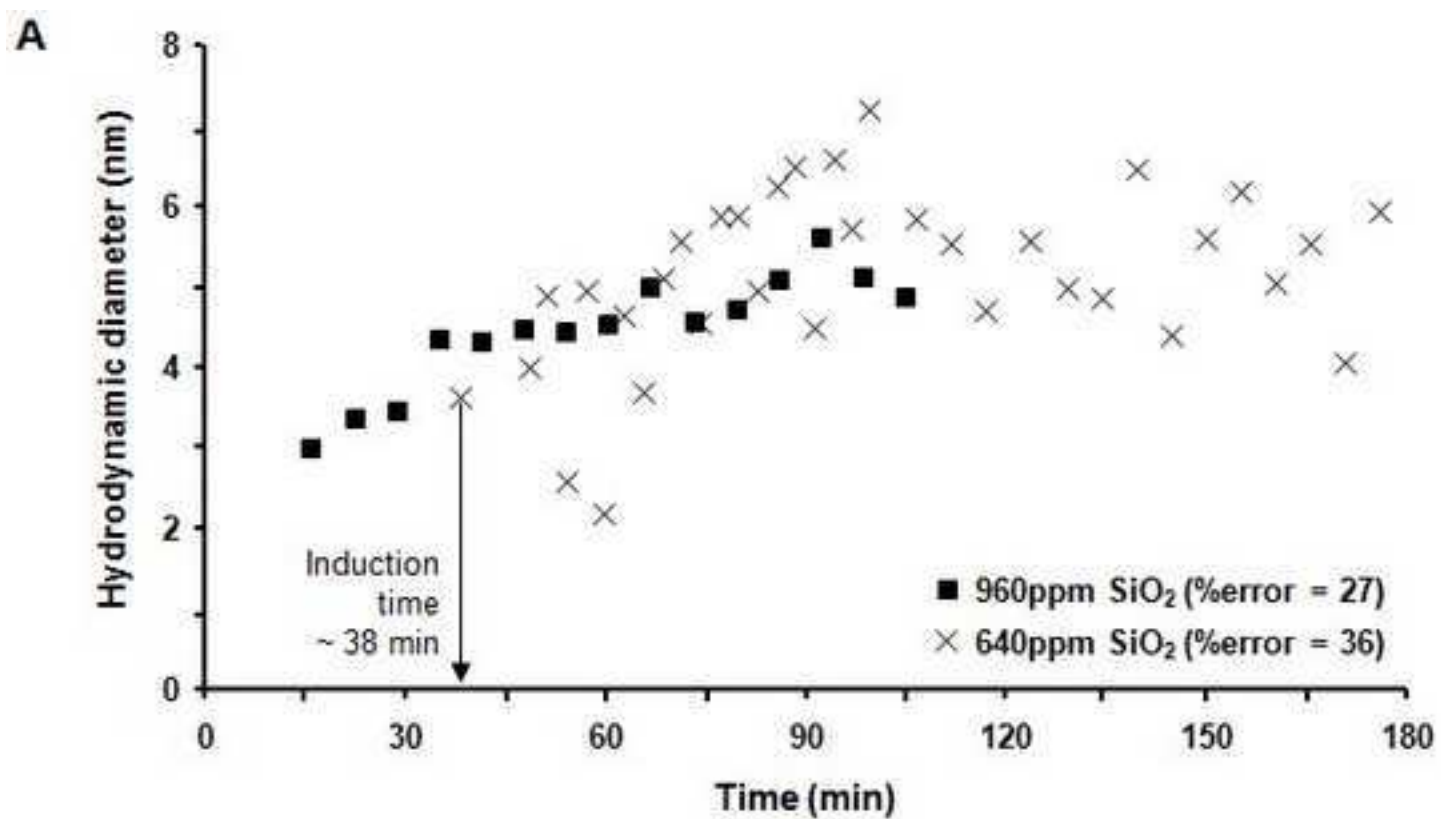
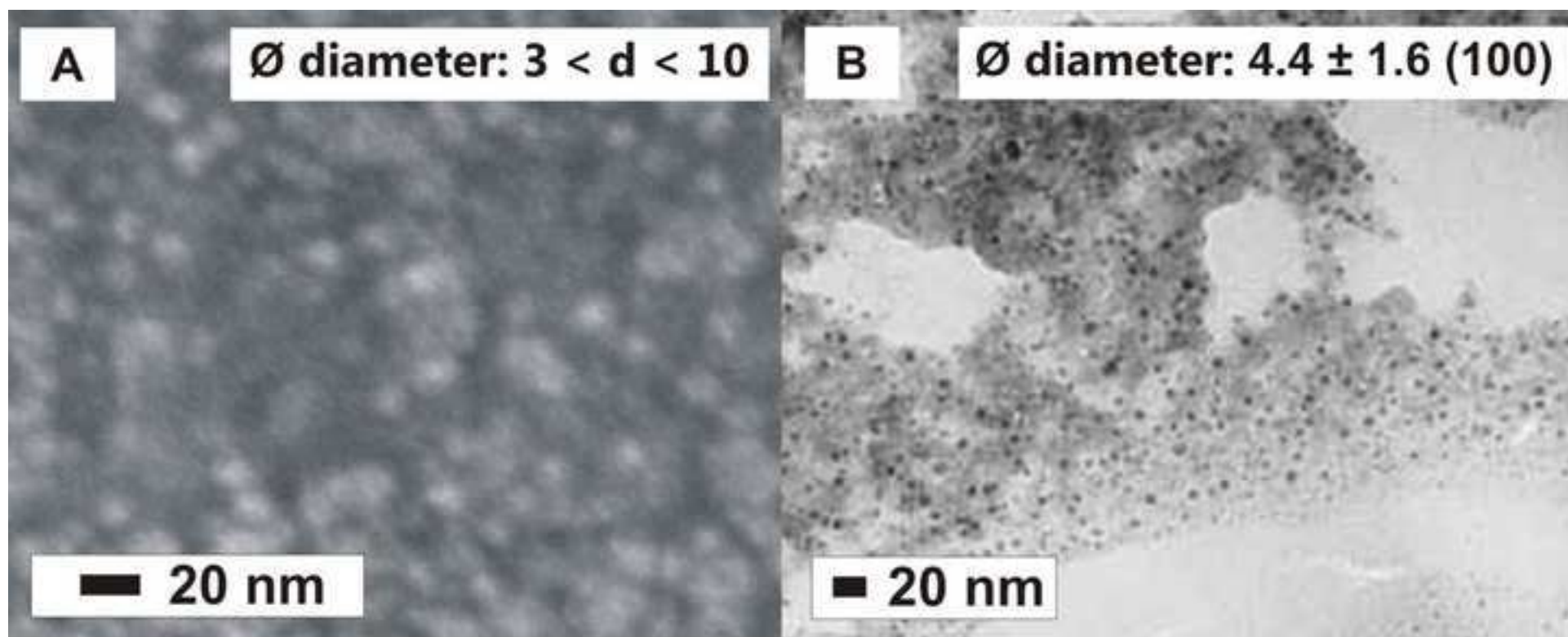


Figure 6
[Click here to download high resolution image](#)



SiO ₂ (ppm)	IS	Time (h)	Particle diameter (nm)		
			SAXS	DLS	TEM
960	0.03	2	6.8 ± 0.2	5.7 ± 2.9	3.2 ± 0.6
		3	7.3 ± 0.2	6.6 ± 3.3	4.4 ± 1.6

Figure 7
[Click here to download high resolution image](#)

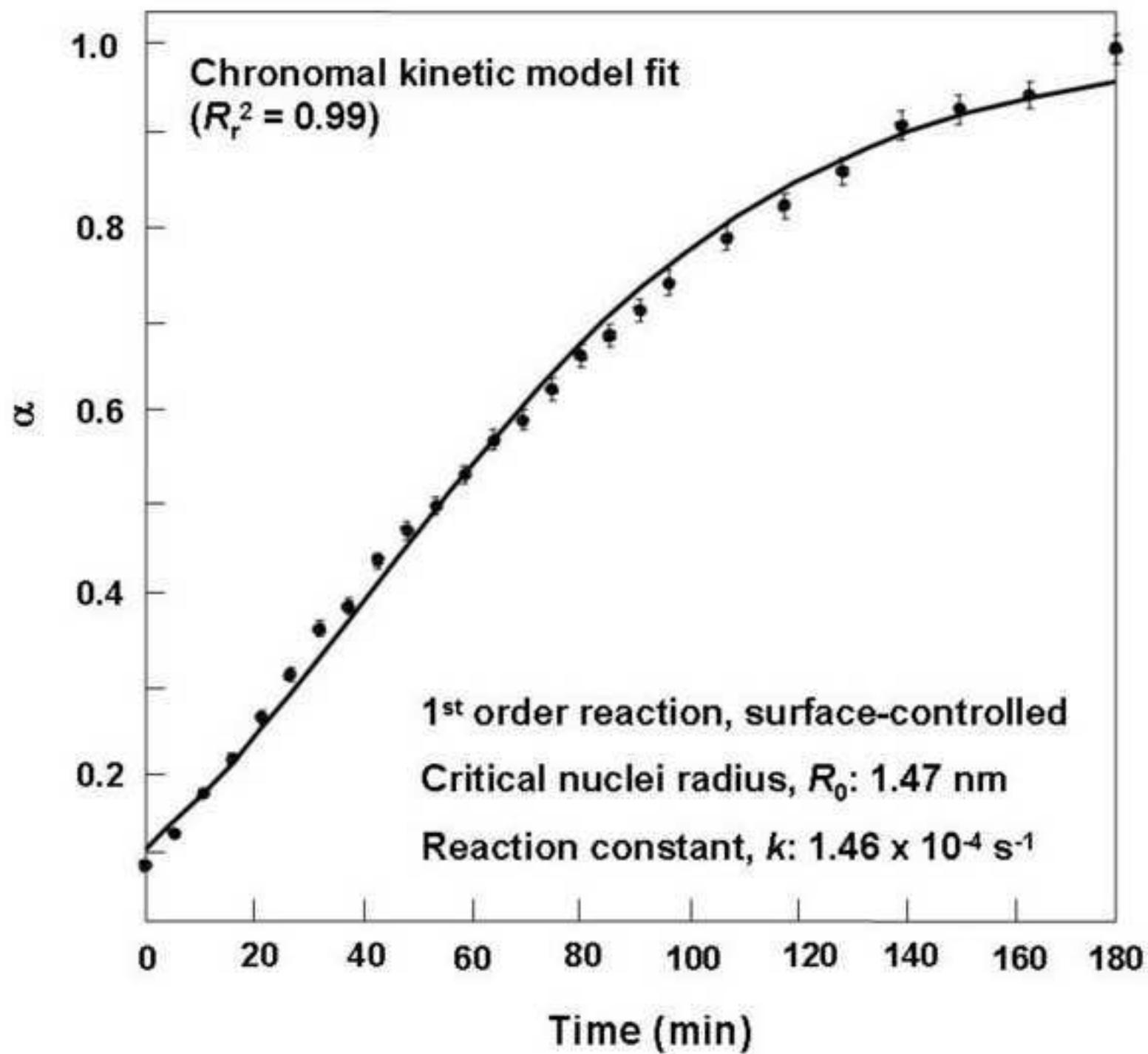


Figure 8
[Click here to download high resolution image](#)

